

Alma Mater Studiorum Università di Bologna  
Archivio istituzionale della ricerca

Attitude Determination from Ellipsoid Observations: A Modified Orthogonal Procrustes Problem

This is the final peer-reviewed author's accepted manuscript (postprint) of the following publication:

*Published Version:*

Modenini, D. (2018). Attitude Determination from Ellipsoid Observations: A Modified Orthogonal Procrustes Problem. JOURNAL OF GUIDANCE CONTROL AND DYNAMICS, 41(10), 2320-2325 [10.2514/1.G003610].

*Availability:*

This version is available at: <https://hdl.handle.net/11585/662968> since: 2019-09-28

*Published:*

DOI: <http://doi.org/10.2514/1.G003610>

*Terms of use:*

Some rights reserved. The terms and conditions for the reuse of this version of the manuscript are specified in the publishing policy. For all terms of use and more information see the publisher's website.

This item was downloaded from IRIS Università di Bologna (<https://cris.unibo.it/>).  
When citing, please refer to the published version.

(Article begins on next page)

This is the final peer-reviewed accepted manuscript of:

**Modenini, D.**

Attitude Determination from Ellipsoid Observations: A Modified  
Orthogonal Procrustes Problem

in: JOURNAL OF GUIDANCE CONTROL AND DYNAMICS, Volume: 41 Issue: 10 Pages: 2320-2325

The final published version is available online at:

<https://doi.org/10.2514/1.G003610>

**Rights / License:**

The terms and conditions for the reuse of this version of the manuscript are specified in the publishing policy. For all terms of use and more information see the publisher's website.

*This item was downloaded from IRIS Università di Bologna (<https://cris.unibo.it/>)*

***When citing, please refer to the published version.***

# **Attitude determination from ellipsoid observations: a modified orthogonal Procrustes problem**

D. Modenini,\*

*Research Fellow, Department of Industrial Engineering, University of Bologna, via Fontanelle 40, 47121, Forlì,  
Italy.*

---

\* Research Fellow, Department of Industrial Engineering (DIN), University of Bologna, via Fontanelle 40, 47121, Forlì, Italy.

Published on Journal of Guidance Control and Dynamics <https://arc.aiaa.org/doi/abs/10.2514/1.G003610>

## I.Introduction

The determination of the attitude from a set of vector observations is a recurrent problem for spacecrafts and aerial vehicles, in general. As such, it has been extensively studied for many decades, leading to several solution methods. Perhaps the most popular formulation for the static attitude determination problem is the one in the form of a least squares minimization, due to Grace Wahba [1]. Finding the attitude matrix minimizing Wahba's loss function has been shown to be equivalent to an orthogonal Procrustes problem, which can be solved through the singular value decomposition method [2].

In this note we address a related problem, which is the one of attitude determination from imaged ellipsoids. Apart from the general interest from a theoretical viewpoint, this topic is of practical application for spacecraft attitude determination, as many platforms are equipped with horizon sensors detecting the limb of an ellipsoid-like body, the Earth. Typically, such sensors are employed to provide a unit vector – the nadir direction – which is then combined with (at least) another observed direction to compute the full attitude [3]. When imaging a spherical target, a unit vector measurement is the best we can aim to, due to axial-symmetry. If instead the target is an ellipsoid of known shape and known orientation, then the rotation about nadir can also be computed, thus constraining the full attitude: the analytical solution to such problem is the main objective of this work.

Horizon sensors are certainly not the only optical-based attitude determination method: stars can also be used as targets for this purpose ([4], [5]). Indeed, star trackers are known to provide arcsecond level accuracy making them the most accurate attitude sensors to date, with extensive flight heritage. Another approach is the one exploiting images of partially overlapping portions of the target surface. These images are processed in pairs through the extraction and matching of coherent features, to solve for the frame-to-frame relative transformation, which is known as the image registration problem [6]. What differs between the above methods is the size of the target with respect to the camera Field of View (FoV). Different image processing techniques are required to extract useful information from an image of the target, depending whether it occupies i) a very small fraction of the FoV, ii) a large portion of the FoV, or iii) if it is much larger than the FoV. In such cases the image processing usually consists of centroids extraction, limb detection, or features extraction, respectively. If star trackers fall under category i) and the application in [6] under iii), the method presented herein belongs to case ii).

The task of computing the attitude of a camera with respect to its target can be considered as the dual of the optical navigation problem: the former aims to provide an estimate of the relative position between the spacecraft

and an imaged planetary target, assuming the attitude is known. Here we deal with the opposite situation, i.e. estimating the attitude when the relative position is known. We will show that, exploiting some analytical results available for the perspective projection of an ellipsoid, the attitude determination problem boils down to a quite simple relation, closely resembling an orthogonal Procrustes problem.

This note is organized as follows: first, we recall the mathematical background of pinhole projective transformations. Then, we formulate the problem of attitude determination from imaged ellipsoids as a least squares minimization, in terms of a modified orthogonal Procrustes problem. A closed form solution to such a problem is given, making use of matrix factorizations. Finally, the performance of the algorithm is tested through numerical simulations on synthetically generated images.

## II. Mathematical Formulation

We adopt a standard projective camera model, for which a point in space with coordinates  $\tilde{\mathbf{x}} = [x \ y \ z]^T$  maps on the image plane (Fig. 1) according to the linear transformation [7]:

$$\mathbf{x} = \mathbf{K}\tilde{\mathbf{x}} \quad (1)$$

In Eq. (1),  $\mathbf{K}$  is the intrinsic camera matrix: for an ideal pinhole camera having optical axis aligned with  $z$ , and the  $x$ -

$y$  plane parallel to the image sensor array,  $\mathbf{K} = \begin{bmatrix} f & 0 & 0 \\ 0 & f & 0 \\ 0 & 0 & 1 \end{bmatrix}$ ,  $f$  being the focal length;  $\mathbf{x} = [fx \ fy \ z]^T$  is the vector of

homogeneous image plane coordinates<sup>2</sup>.

The transformation from the homogeneous 4-D coordinates<sup>3</sup> of a point in world frame,  $\mathbf{x}_w = [x \ y \ z \ 1]^T$ , to the in-homogeneous coordinates in camera frame ( $\tilde{\mathbf{x}}_c$ ), follows as:

$$\tilde{\mathbf{x}}_c = \mathbf{R}[\mathbf{I} \ \mathbf{t}_w]\mathbf{x}_w \quad (2)$$

Or, combining Eq.(1) and (2):

$$\mathbf{x} = \mathbf{K}\mathbf{R}[\mathbf{I} \ \mathbf{t}_w]\mathbf{x}_w \quad (3)$$

which relates the four-dimensional homogeneous coordinates of a point in space, expressed in the camera frame, to its three-dimensional homogeneous projection on the image plane. In other words,  $\mathbf{x}$  are points in the camera sensor

---

<sup>2</sup> The homogeneous coordinates of a point in the image plane are represented by the equivalence classes of coordinate triples, where two triples are equivalent when they differ by a common multiple.

<sup>3</sup> The homogeneous coordinates of a point in the 3D space are represented by the equivalence classes of coordinate quadruples, where two quadruples are equivalent when they differ by a common multiple. The *tilde* symbol is used in this Note to distinguish inhomogeneous coordinates of a point in space from the homogeneous ones.

array, which can be directly related to the image pixels. In Eq. (3),  $\mathbf{R}$  is the attitude (rotation) matrix mapping from the world frame to camera (body) frame, and  $\mathbf{t}_w$  is the translation vector from the camera center to the origin of the coordinate system, expressed in world coordinates. Therefore, Eq. (3) combines the roto-translation transformation from the world frame to the camera frame with the projective transformation.

Without loss of generality, we consider an ellipsoid centered in the origin of the world frame, with axes aligned to those of the world frame. The points on its surface are described through the homogeneous quadric equation:

$$\mathbf{x}_w^T \mathbf{Q} \mathbf{x}_w = 0 \quad (4)$$

where:

$$\mathbf{Q} = \begin{bmatrix} 1/a^2 & 0 & 0 & 0 \\ 0 & 1/b^2 & 0 & 0 \\ 0 & 0 & 1/c^2 & 0 \\ 0 & 0 & 0 & -1 \end{bmatrix} \quad (5)$$

and  $a$ ,  $b$  and  $c$  are the semi-axes, which for now are assumed to be distinct<sup>4</sup>. All the subsequent analysis will rely on the following known result from perspective geometry [7]: under the transformation  $\mathbf{T} = \mathbf{R}[\mathbf{I} \quad \mathbf{t}_w]$ , the quadric  $\mathbf{Q}$  transforms to a conic  $\mathbf{C}$  (i.e. a 3x3 symmetric matrix) on the image plane, according to:

$$\mathbf{C}^* \propto \mathbf{K} \mathbf{T} \mathbf{Q}^* \mathbf{T}^T \mathbf{K}^T \quad (6)$$

where  $*$  superscript stands for adjoint, which in case of an ellipsoid equates to the inverse, thus  $\mathbf{Q}^* = \mathbf{Q}^{-1}$  and  $\mathbf{C}^* = \mathbf{C}^{-1}$ . The inverse quadric (conic) is the locus of the planes (lines) tangent to the original quadric (conic). In practice, Eq. (6) shows a well-known result, i.e. that when imaging an ellipsoid, we retrieve an ellipse<sup>5</sup>.

Eq. (6) is valid up to a scale factor, since the symmetric matrix  $\mathbf{C}$  represents a conic in homogeneous coordinates which, in turn, is fully determined by 5 independent parameters. Therefore, the 3x3 matrix representation of a conic is invariant to a scale factor. If we define  $\mathbf{C}_{im}^* = \mathbf{K}^{-1} \mathbf{C}^* \mathbf{K}^{-T}$ , we may rewrite Eq. (6) as:

$$\alpha \mathbf{C}_{im}^* = \mathbf{T} \mathbf{Q}^* \mathbf{T}^T \quad (7)$$

with  $\alpha$  being an unknown constant to be determined.  $\mathbf{C}_{im}$  and  $\mathbf{C}_{im}^*$  are computed starting from the coefficients of the ellipse quadratic equation:

$$Ax^2 + Bxy + Cy^2 + Dx + Ey + G = 0 \quad (8)$$

---

<sup>4</sup> Later in the manuscript, the analysis will be tailored for the special cases of a sphere and a spheroid, such as the Earth.

<sup>5</sup> The geometric interpretation is that the ellipse results from the intersection of the cone tangent to the ellipsoid and whose vertex is lying on the camera center, with the image plane.

In particular, for an ideal pinhole camera having intrinsic matrix  $\mathbf{K} = \begin{bmatrix} f & 0 & 0 \\ 0 & f & 0 \\ 0 & 0 & 1 \end{bmatrix}$ , it follows:

$$\mathbf{C}_{im} = \begin{bmatrix} Af^2 & \frac{Bf^2}{2} & \frac{Df}{2} \\ \frac{Bf^2}{2} & Cf^2 & \frac{Ef}{2} \\ \frac{Df}{2} & \frac{Ef}{2} & G \end{bmatrix} \quad (9)$$

and:

$$\mathbf{C}_{im}^* = \begin{bmatrix} \frac{E^2 - 4CG}{f^2k} & \frac{2BG - DE}{f^2k} & \frac{2CD - BE}{fk} \\ \frac{2BG - DE}{f^2k} & \frac{D^2 - 4AG}{f^2k} & \frac{2AE - BD}{fk} \\ \frac{2CD - BE}{fk} & \frac{2AE - BD}{fk} & \frac{B^2 - 4AC}{k} \end{bmatrix} \quad (10)$$

$$k = GB^2 - BDE + CD^2 + AE^2 - 4ACG$$

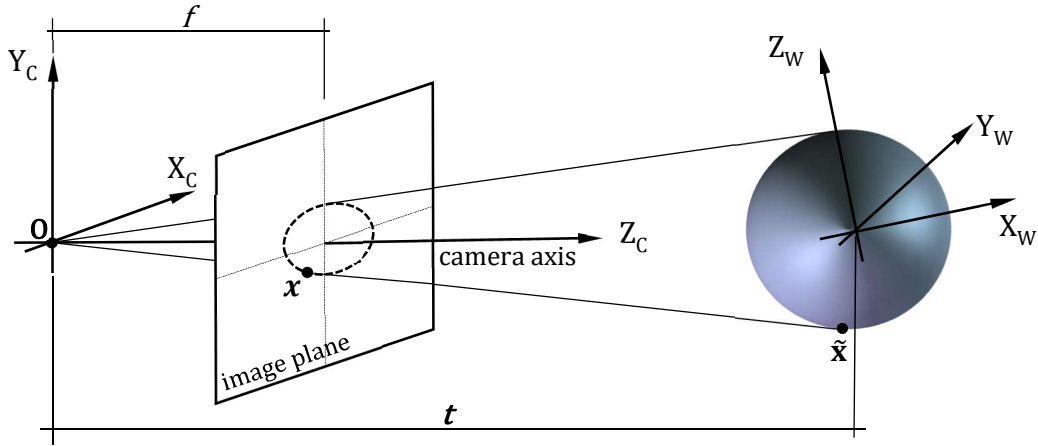


**Fig. 1 Schematic of the pinhole camera model. A point in space,  $x$ , is mapped to the point on the image plane,  $x$ , where a line joining  $x$  to the center of projection,  $O$ , meets the image plane.  $O$  is also assumed as the center of the camera fame.**

Since the inverse quadric matrix  $\mathbf{Q}^*$  admits the block-diagonal decomposition  $\mathbf{Q}^* = \begin{bmatrix} \mathbf{Q}_3^* & \mathbf{0} \\ \mathbf{0} & -1 \end{bmatrix}$ , the rotational and translational part of the transformation in Eq. (7) can be decoupled, according to:

$$\alpha \mathbf{C}_{im}^* = \mathbf{R}(\mathbf{Q}_3^* - \mathbf{t}_w \mathbf{t}_w^T) \mathbf{R}^T \quad (11)$$

where we used the notation  $\mathbf{Q}_3^* = \mathbf{Q}^*(1:3,1:3)$ . The camera attitude estimation problem reduces then to the determination of  $\mathbf{R}$  from the knowledge of  $\mathbf{C}_{im}^*$  and  $\mathbf{Q}_3^*$  and the relative position  $\mathbf{t}_w$ . If we denote matrix  $\mathbf{B}^* = (\mathbf{Q}_3^* - \mathbf{t}_w \mathbf{t}_w^T)$ , Eq. (11) can be rewritten as:

$$\mathbf{R}\mathbf{B}^*\mathbf{R}^T = \alpha\mathbf{C}_{im}^* \quad (12)$$

which means that  $\mathbf{B}^*$  and  $\alpha\mathbf{C}_{im}^*$  are similar matrices. The determination of the scaling factor  $\alpha$  is straightforward by taking the trace of Eq. (12):

$$\text{tr}(\mathbf{R}\mathbf{B}^*\mathbf{R}^T) = \text{tr}(\mathbf{B}^*) = \alpha\text{tr}(\mathbf{C}_{im}^*) \quad (13)$$

Thus:

$$\alpha = \text{tr}(\mathbf{B}^*)/\text{tr}(\mathbf{C}_{im}^*) \quad (14)$$

That is, the inverse ellipse matrix is scaled to have its trace matching the one of  $\mathbf{B}^*$  which, in turn, depends on the size of the imaged ellipsoid and on the position of the observing spacecraft.

To solve for the attitude matrix  $\mathbf{R}$ , we make use of the spectral theorem for symmetric matrices to write:

$$\alpha\mathbf{C}_{im}^* = \mathbf{V}\mathbf{D}_C\mathbf{V}^T; \mathbf{B}^* = \mathbf{W}\mathbf{D}_B\mathbf{W}^T \quad (15)$$

with  $\mathbf{V}$ ,  $\mathbf{W}$  orthogonal matrices. However, since  $\mathbf{B}^*$  and  $\alpha\mathbf{C}_{im}^*$  are similar,  $\mathbf{D}_C = \mathbf{D}_B = \mathbf{D}$ . Now, it is easy to verify that by setting

$$\mathbf{R} = \mathbf{V}\mathbf{W}^T \quad (16)$$

Eq. (12) is satisfied. Actually, any matrix of the form:

$$\mathbf{R} = \mathbf{V}\mathbf{P}\mathbf{W}^T \quad (17)$$

with  $\mathbf{P} = \text{diag}\{\pm 1 \pm 1 \pm 1\}$  will be a solution, too. The above holds, however, only in an ideal case. Indeed, because of measurement errors,  $\mathbf{D}_C$  will differ from  $\mathbf{D}_B$  (though hopefully not much); nevertheless, we can still employ Eq. (16) as an estimator for  $\mathbf{R}$ . This way we would have:

$$\alpha\mathbf{C}_{im}^*\mathbf{R} - \mathbf{R}\mathbf{B}^* = \mathbf{V}(\mathbf{D}_C - \mathbf{D}_B)\mathbf{W}^T \neq \mathbf{0} \quad (18)$$

We will prove that Eq. (17) provides an optimal attitude solution in a least squares sense, through the following:

*Theorem. Solution to a modified orthogonal Procrustes problem*

Given two symmetric matrices  $\mathbf{A}$  and  $\mathbf{B}$ , admitting the spectral decomposition:

$$\mathbf{A} = \mathbf{U}\mathbf{D}_A\mathbf{U}^T, \mathbf{B} = \mathbf{V}\mathbf{D}_B\mathbf{V}^T \quad (19)$$

Then the solution to the following modified orthogonal Procrustes problem:



$$\min_{\mathbf{R}} \|\mathbf{AR} - \mathbf{RB}\|_F^2 \quad \text{subject to } \mathbf{R}^T \mathbf{R} = \mathbf{I} \quad (20)$$

is given by any of the matrices:

$$\mathbf{R} = \mathbf{UPV}^T \quad (21)$$

provided that the eigenvalues are arranged in the same order relative to each other, and  $\mathbf{P}$  denotes the family of eight orthogonal matrices:

$$\mathbf{P} = \begin{bmatrix} \pm 1 & 0 & 0 \\ 0 & \pm 1 & 0 \\ 0 & 0 & \pm 1 \end{bmatrix} \quad (22)$$

The proof is given in Appendix A.

Eq. (20) is a variant of the well-known orthogonal Procrustes problem, which provides the attitude matrix solution to Wahba's problem with multiple vector observations [8]. The eight possible solutions given by Eq. (21), provide all the same residual Frobenius norm. We are interested, however, only in those generated by proper rotation matrices, i.e. for which  $\det(\mathbf{R})=1$ . For example, if we assume  $\det(\mathbf{UV}^T) = 1$ , then

$$\det(\mathbf{UPV}^T) = \begin{cases} = +1 \text{ for } \text{diag}(\mathbf{P}) = \begin{bmatrix} +1, +1, +1 \\ -1, -1, +1 \\ +1, -1, -1 \\ -1, +1, -1 \end{bmatrix} \\ = -1 \text{ for } \text{diag}(\mathbf{P}) = \begin{bmatrix} +1, +1, -1 \\ +1, -1, +1 \\ -1, +1, +1 \\ -1, -1, -1 \end{bmatrix} \end{cases} \quad (23)$$

Therefore, there is a four-fold ambiguity in the solution, with the four candidate  $\mathbf{P}$  matrices being the ones for which the sign of the product of the diagonal elements equates the sign of  $\det(\mathbf{UV}^T)$ . The ambiguity can be reduced noting that, out of the four possible attitude matrices, only two corresponds to the camera pointing towards the ellipsoid, i.e. for which the sign of the third components of the nadir vector expressed in camera frame:

$$(\mathbf{R}\mathbf{t}_w)^T \begin{bmatrix} 0 \\ 0 \\ 1 \end{bmatrix} = t_{c,3} \quad (24)$$

is positive. Then, there will be a two-fold ambiguity left in the solution that cannot be resolved, which is a direct consequence of the symmetry of the ellipsoid surface with respect to its meridian planes. The undistinguishable attitude configurations are easy to visualize when considering a nadir-pointing camera, as they differ for a  $180^\circ$  rotation about the optical axis (see Fig. 2). To select the correct solution some additional independent information is needed, e.g. past attitude history or angular information obtained from other sensors.

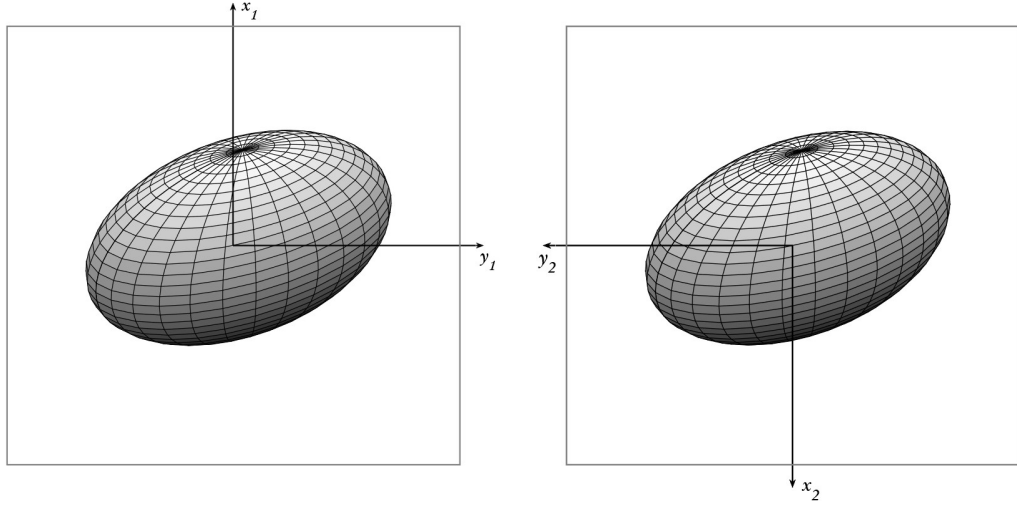


**Fig. 2 Schematic view of two indistinguishable attitude when imaging an ellipsoid: camera 1 (left panel) and camera 2 (right panel) would capture the same image, despite having different orientations.**

#### A. Summary of the algorithm and implementation considerations

The attitude determination algorithm from imaged ellipsoids can be summarized in the following steps:

1. Detect the limb from the gathered image.
2. Fit an ellipse to the detected limb pixels' coordinates.
3. Compute matrix  $\mathbf{C}_{im}^*$  from the ellipse coefficients according to Eq. (10).
4. Given the camera position  $\mathbf{t}_w$  and the target ellipsoid semi-axes, compute matrix  $\mathbf{B}^*$  and scale matrix  $\mathbf{C}_{im}^*$  according to Eq. (14).
5. Compute matrices  $\mathbf{W}$  and  $\mathbf{V}$ , collecting the eigenvectors of  $\mathbf{B}^*$  and  $\mathbf{C}_{im}^*$ .
6. Choose the four  $\mathbf{P}_i$  matrices from Eq. (23) having determinant of the same sign than the one of the product  $\mathbf{VW}^T$ , such that  $\mathbf{R}_i = \mathbf{V}\mathbf{P}_i\mathbf{W}^T$  provides a proper rotation matrix.
7. Select the only two possible attitude solutions corresponding to the camera pointing towards the target, by checking the sign of the third component of the nadir vector expressed in camera frame.

Points 1 and 2 would deserve some extensive considerations *per se*, however, since they are not the core of this work, we will not pursue such topics any further. It will suffice to say that many methods are available in the literature, for both image edge detections and ellipse fitting (see, e.g., [9], [10], [11]). For a discussion on edge detection applied to images of celestial bodies for optical navigation, the reader is referred to [12].

Concerning step 5, it is interesting to note that, as we deal with 3x3 symmetric matrices, the eigen-decomposition admits an analytical solution. This can be implemented very efficiently and without resorting to iterative numerical schemes. Indeed, the eigenvalues  $\lambda_i$  of a generic 3x3 matrix  $\mathbf{A}$  can be computed as the solution of a third order polynomial using Cardano's formula, while the eigenvectors  $\mathbf{v}_i$  are obtained from cross products [13]:

$$\mathbf{v}_i = \left( \mathbf{A}^1 - \lambda_i \begin{bmatrix} 1 \\ 0 \\ 0 \end{bmatrix} \right) \times \left( \mathbf{A}^2 - \lambda_i \begin{bmatrix} 0 \\ 1 \\ 0 \end{bmatrix} \right) \quad (25)$$

where the superscript indexes denote matrix columns.

In many practical applications, it is of interest to determine the attitude of the camera with respect to a frame related the local vertical. One frame which is commonly employed is the NED (North-East-Down) one. We can of course reformulate the above algorithm to solve for the attitude with respect to such a frame, as follows. First, we write the attitude matrix  $\mathbf{R}$  as the combination of two rotations:

$$\mathbf{R} = \mathbf{R}_{c/n} \mathbf{R}_{n/w} \quad (26)$$

Where  $\mathbf{R}_{n/w}$  is the rotation matrix from the world frame to NED frame, and  $\mathbf{R}_{c/n}$  is the rotation matrix from NED to camera frame. Upon substitution of Eq. (26), Eq. (11) can be rewritten as:

$$\alpha \mathbf{C}_{im}^* = \mathbf{R}_{c/n} \mathbf{R}_{n/w} (\mathbf{Q}_3^* - \mathbf{t}_w \mathbf{t}_w^T) \mathbf{R}_{n/w}^T \mathbf{R}_{c/n}^T = \mathbf{R}_{c/n} (\mathbf{Q}_n^* - \mathbf{t}_n \mathbf{t}_n^T) \mathbf{R}_{c/n}^T = \mathbf{R}_{c/n} \left( \mathbf{Q}_n^* - \begin{bmatrix} 0 & 0 & 0 \\ 0 & 0 & 0 \\ 0 & 0 & \rho^2 \end{bmatrix} \right) \mathbf{R}_{c/n}^T \quad (27)$$

where  $\mathbf{Q}_n^* = \mathbf{R}_{n/w} \mathbf{Q}_3^* \mathbf{R}_{n/w}^T$ ,  $\mathbf{t}_n = \mathbf{R}_{n/w} \mathbf{t}_w = [0 \ 0 \ \rho]^T$ ,  $\rho$  being the range from the camera to the ellipsoid center.

Then, re-defining  $\mathbf{B}_n^* = \mathbf{Q}_n^* - \begin{bmatrix} 0 & 0 & 0 \\ 0 & 0 & 0 \\ 0 & 0 & \rho^2 \end{bmatrix}$ , the solution algorithm can now be applied to determine the attitude with

respect to NED frame. With respect to the previous definition of  $\mathbf{B}^*$ , we note that the dependency on the relative position between the camera and the target is now found inside the definition of the ellipsoid matrix  $\mathbf{Q}_n^*$ , through the computation of  $\mathbf{R}_{n/w}$ .

### B. Special case 1: imaging a sphere

When imaging a sphere, the full attitude cannot be retrieved. If we parametrize the NED relative attitude with a 3-2-1 ( $\psi$ =yaw,  $\vartheta$ =pitch,  $\varphi$ =roll) Euler angles sequence, the yaw angle is clearly unobservable due to spherical-symmetry. Consequently, the estimated  $\mathbf{R}_{c/n}$  matrix will not approach the true one in general, even in an ideal error-

free scenario. However, in this case the third column of  $\mathbf{R}_{c/n}$  only matters, which fully determines the observable pitch-roll angles through:

$$\mathbf{R}_{c/n}^3 = \begin{bmatrix} -\sin(\vartheta) \\ \sin(\varphi)\cos(\vartheta) \\ \cos(\varphi)\cos(\vartheta) \end{bmatrix} \quad (28)$$

apart from the signs, which should be adjusted as outlined at the end of Section II. On the other hand, imaging a sphere does not require the complete knowledge of the spacecraft position, as only the range is needed. This intuitive result is apparent from Eq. (27), since for a spherical target of radius  $r$ ,  $\mathbf{Q}_n^* = r^2 \mathbf{I}$  regardless of the point of observation (i.e. regardless of  $\mathbf{R}_{n/w}$ ), and  $\mathbf{B}_n^*$  depends on the range  $\rho$  only.

### C. Special case 2: imaging a spheroid

The most favorable condition to fully determine the attitude using the present algorithm is when the target is a triaxial ellipsoid. However, many celestial bodies are spheroids, i.e. ellipsoids of revolution. In this case, the capability of detecting the yaw angle depends on the observation point: whenever the local vertical is aligned to the axis of revolution, then the same symmetry problem outlined in Section II.B. for the sphere occurs. In general, we may expect that the accuracy of the yaw angle determination worsens when approaching such a condition, as will be shown by the numerical simulations in the next section. The detectability of the orientation about nadir is also degraded when the difference between the polar and equatorial semi-axes gets smaller: unfortunately, the usual celestial target for a spacecraft horizon sensor is the Earth, which has a very low flattening ( $\approx 1/298$ ).

The expected yaw-angle accuracy in such a practical scenario is quite low, and one may argue whether to use it or disregard it. Nevertheless, the present formulation remains useful, as the full information available from the target shape is exploited in the computation of the remaining detectable angles, roll and pitch.

## III. Numerical Simulation

The proposed method was tested through numerical simulations using MATLAB 3D scenes control tool. To this end, we plotted an ellipsoid with given axes and specified camera location, orientation and field of view. Then, we generated some images at a resolution 1024x1024 pixels with 8-bit grey levels and corrupted them with additive gaussian noise having standard deviation equal to 4 digital levels. The aim of this analysis is to check the consistency of the algorithm and to assess its potential maximum accuracy, rather than evaluating an application-

dependent error budget. Therefore, no other error sources were considered. In particular, we left out of the analysis one known error affecting horizon sensors, which is the shift of the apparent planetary limb due to the presence of an atmosphere. Indeed, most horizon sensors consists of far infrared detectors, as the highest limb stability is found in the CO<sub>2</sub> absorption wavelengths (14-16  $\mu\text{m}$ ) [14][15]. Assessing the impact of the atmospheric induced limb shift is quite involved, since it depends on the specific detector implementation and spectral response, as well as the employed atmospheric model; a task which is beyond the scope of this short note. A further simplification adopted in the simulation is the assumption that the entire limb is included in the image: this is an unlikely event, especially for the application scenario of a Low Earth Orbit spacecraft, and it might be overcome using multiple sensor heads.

Generated images were processed using a discrete convolutional operator for limb detection. Then, an ellipse was fitted to the detected limb pixels using the method described in [16]. Finally, the algorithm presented in Section II.A was applied to each image to identify the two admissible attitude solutions. The one closest to the true attitude was retained as the correct one to compute the error in terms of yaw-pitch-roll angles.

Simulations are provided for two scenarios: a) a triaxial ellipsoid with semi-axes 1.0 0.9 and 0.81, and b) an Earth-like spheroid with semi-axes equal to 1.0, 1.0 and  $(1-f)$ ,  $f=1/298$ . The camera attitude was prescribed to be nominally nadir-pointing with some randomly generated, normally distributed off-nadir angles (all of them having mean and standard deviation  $\mu=0^\circ$ ,  $\sigma=3^\circ$ , respectively). Images were gathered at different longitude and latitude, both ranging from  $0^\circ$  to  $90^\circ$ , with  $10^\circ$  of angular step<sup>6</sup>. Sample angular errors are displayed in Fig. 3 and Fig. 4, while mean and *rms* values are collected in Table 1.

The algorithm reaches a  $1-\sigma$  accuracy in pitch and roll of a few arcseconds. As expected, the accuracy for the yaw angle (around boresight) is significantly lower than for the other two angles, a feature commonly encountered in star trackers also. In case of an imaged triaxial ellipsoid, scenario a), the difference is about 1 order of magnitude. For scenario b), the yaw accuracy gets worse, with the associated error shooting up dramatically while approaching the  $90^\circ$  of latitude: the yaw error remains below  $1^\circ$  up to a latitude of about  $70^\circ$ . On the other hand, pitch and roll angles accuracies are only marginally degraded when approaching the symmetry axis.

During the numerical tests, we also tried different convolutional operators for limb detection. It was found that the error curves shape was affected to some extent; however, the features described above, and the overall mean and *rms* error values reported, were practically unchanged.

---

<sup>6</sup> Since an ellipsoid has two symmetry planes, the error patterns repeat periodically outside of the range  $[0^\circ 90^\circ]$ .

**Table 1 Attitude angles estimation errors**

Simulation	Yaw error, arcsec		Pitch error, arcsec		Roll error, arcsec	
scenario	mean	<i>rms</i>	mean	<i>rms</i>	mean	<i>rms</i>
a	3.1	47.8	0.67	2.7	3.4	5.9
b	-43	1814 <sup>7</sup>	0.1	2.2	2.0	10.8

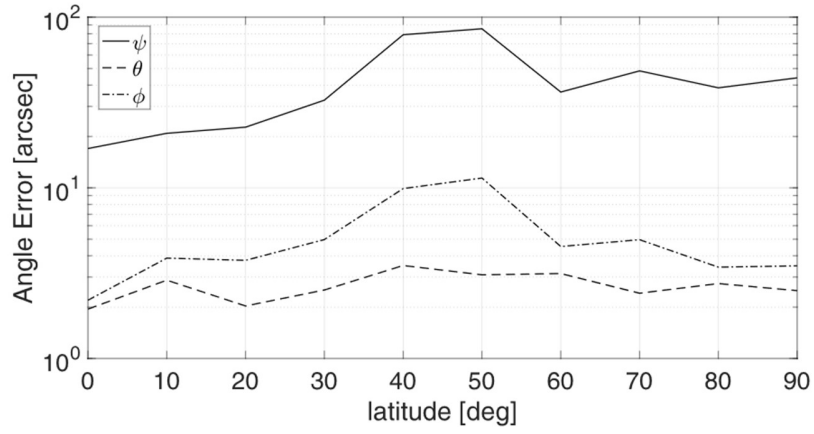
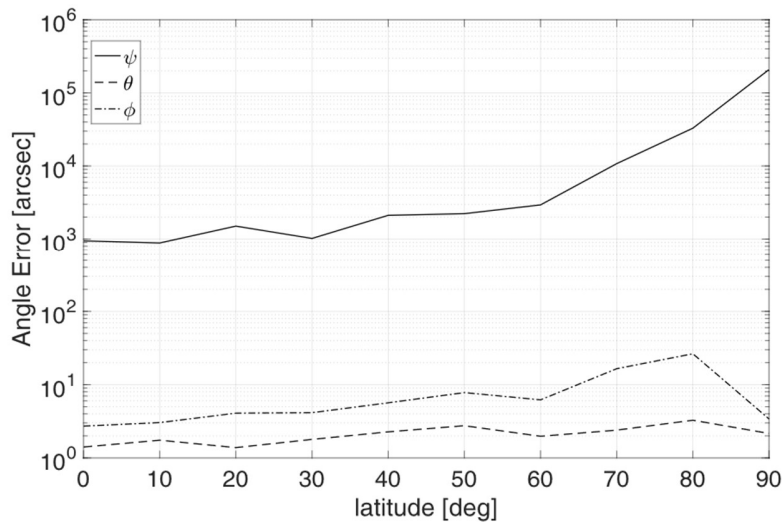


**Fig. 3 Attitude errors as a function of the latitude of observation (*rms* averaged over longitude) for a triaxial ellipsoid (simulation scenario a).**



<sup>7</sup> Yaw error statistics for case b) are computed within a limited latitude range up to 70°.

**Fig. 4 Attitude errors as a function of the latitude of observation (*rms* averaged over longitude) for an Earth-like spheroid (simulation scenario b).**

#### **IV. Conclusion**

In this note we presented an analytical solution to the attitude estimation problem from imaged ellipsoids. This problem is of interest for spacecraft attitude determination using horizon sensors.

Starting from the ellipsoid image, the limb is extracted and fitted to an ellipse. Then, by making use of some analytical results from perspective geometry, the attitude matrix is computed through a modified orthogonal Procrustes problem. The solution, which is optimal in a least squares sense, is given in terms of the spectral decomposition of two symmetric matrices, one collecting the coefficients of the fitted ellipse, the other being the ellipsoid matrix corrected by the relative position between the target and the observer. The proposed formulation has the advantage of accounting for the non-spherical shape of the target to estimate the entire attitude rather than the nadir vector only.

The consistency of the algorithm was assessed through numerical simulations with synthetically generated images. Results show that the maximum achievable  $1\sigma$  accuracy are in the order of few arcseconds for pitch and roll angles, and one order of magnitude worse for the yaw angle. As expected, for an Earth-like spheroid target with very low flatness, the yaw angle is measurable with even lower accuracy, depending also on the latitude of the observation, with a loss of observability when imaging with the local vertical parallel to the axis of revolution.

When compared to other optical-based attitude determination methods, the present differs on how the information is extracted from the image, i.e. through limb detection and fitting, which is an intermediate option with respect to the centroiding, typical of those cases in which the target is small with respect to the FoV, such as for star trackers, and the features extraction, used in more complex frame-to-frame image registration algorithms.

In conclusion, the proposed attitude determination method looks promising for a horizon sensor implementation. Nevertheless, future efforts are required to address its practical applicability, including a sensitivity analysis of the solution to uncertain parameters and a realistic error budget under representative operational scenarios.

## V. Appendix

Given two symmetric matrices  $\mathbf{A}$  and  $\mathbf{B}$ , we want to find the matrix (or matrices)  $\mathbf{R} = [r_{i,j}]$ , such that:

$$\min_{\mathbf{R}} \|\mathbf{AR} - \mathbf{RB}\|_F^2 \quad \text{subject to } \mathbf{R}^T \mathbf{R} = \mathbf{I} \quad (29)$$

Since:

$$\begin{aligned} \|\mathbf{AR} - \mathbf{RB}\|_F^2 &= \text{trace}[(\mathbf{AR} - \mathbf{RB})^T (\mathbf{AR} - \mathbf{RB})] \\ &= \text{trace}(\mathbf{A}^2) + \text{trace}(\mathbf{B}^2) - \text{trace}(\mathbf{R}^T \mathbf{ARB}) - \text{trace}(\mathbf{BR}^T \mathbf{AR}) \\ &= \text{trace}(\mathbf{A}^2) + \text{trace}(\mathbf{B}^2) - 2 \text{trace}(\mathbf{R}^T \mathbf{ARB}) \end{aligned} \quad (30)$$

The problem is equivalent to the one of maximizing  $\text{trace}(\mathbf{R}^T \mathbf{ARB})$ . Consider the spectral decomposition for  $\mathbf{A}$  and

$\mathbf{B}$ :  $\mathbf{A} = \mathbf{UD}_A \mathbf{U}^T$  and  $\mathbf{B} = \mathbf{VD}_B \mathbf{V}^T$ :

Then:

$$\text{trace}(\mathbf{R}^T \mathbf{ARB}) = \text{trace}(\mathbf{R}^T \mathbf{UD}_A \mathbf{U}^T \mathbf{RVD}_B \mathbf{V}^T) = \text{trace}(\mathbf{V}^T \mathbf{R}^T \mathbf{UD}_A \mathbf{U}^T \mathbf{RVD}_B) = \text{trace}(\mathbf{Z}^T \mathbf{D}_A \mathbf{ZD}_B) \quad (31)$$

Where we denoted with  $\mathbf{Z} = [z_{i,j}]$  the orthogonal matrix:  $\mathbf{U}^T \mathbf{R} \mathbf{V}$ . We assume that the decomposition of  $\mathbf{A}$  and  $\mathbf{B}$  is ordered such that the elements of  $\mathbf{D}_A = \text{diag}\{\sigma_{A,1}, \sigma_{A,2}, \sigma_{A,3}\}$  and  $\mathbf{D}_B = \text{diag}\{\sigma_{B,1}, \sigma_{B,2}, \sigma_{B,3}\}$  are both arranged in descending order, i.e.:  $\sigma_{A,1} \geq \sigma_{A,2} \geq \sigma_{A,3}$  and  $\sigma_{B,1} \geq \sigma_{B,2} \geq \sigma_{B,3}$ . Next, we will show that:

$$\text{trace}(\mathbf{Z}^T \mathbf{D}_A \mathbf{ZD}_B) \leq \text{trace}(\mathbf{PD}_A \mathbf{PD}_B) = \text{trace}(\mathbf{D}_A \mathbf{D}_B) \quad (32)$$

with  $\mathbf{P}$  defined in Eq. (22). Then the theorem will be proved, as  $\mathbf{R} = \mathbf{UPV}^T$ , would be a minimizer, leading to  $\mathbf{Z} = \mathbf{P}$ .

To this end, let us define the matrix:  $\mathbf{M} = [m_{i,j}] = \mathbf{Z}^T \mathbf{D}_A \mathbf{Z}$ , then:

$$\text{trace}(\mathbf{Z}^T \mathbf{D}_A \mathbf{ZD}_B) = \text{trace}(\mathbf{MD}_B) = \sum_i \sigma_{B,i} m_{i,i} = \sum_i \sigma_{B,i} \left( \sum_j \sigma_{A,j} z_{j,i}^2 \right) \quad (33)$$

Then, we seek for the maximum of Eq. (33) over  $i$  by maximizing each addend individually. The first term,  $i=1$ , becomes:

$$\sigma_{B,1} (\sigma_{A,1} z_{1,1}^2 + \sigma_{A,2} z_{2,1}^2 + \sigma_{A,3} z_{3,1}^2) = \sigma_{B,1} \sigma_{A,1} \left( z_{1,1}^2 + \frac{\sigma_{A,2}}{\sigma_{A,1}} z_{2,1}^2 + \frac{\sigma_{A,3}}{\sigma_{A,1}} z_{3,1}^2 \right) \quad (34)$$

If we substitute  $z_{1,1}^2 = 1 - z_{2,1}^2 - z_{3,1}^2$ , we get:

$$\sigma_{B,1} \sigma_{A,1} \left( 1 + \left( \frac{\sigma_{A,2}}{\sigma_{A,1}} - 1 \right) z_{2,1}^2 + \left( \frac{\sigma_{A,3}}{\sigma_{A,1}} - 1 \right) z_{3,1}^2 \right) \leq \sigma_{B,1} \sigma_{A,1} \quad (35)$$



which clearly has a maximum for  $z_{2,1} = 0, z_{3,1} = 0$ ; thus  $z_{1,1} = \pm 1$ . This in turn implies also  $z_{1,2} = 0, z_{1,3} = 0$ , since  $\mathbf{Z}$  is orthogonal.

For the term  $i=2$  it holds:

$$\sigma_{B,2}(\sigma_{A,1}z_{1,2}^2 + \sigma_{A,2}z_{2,2}^2 + \sigma_{A,3}z_{3,2}^2) = \sigma_{B,2}\sigma_{A,2}\left(z_{2,2}^2 + \frac{\sigma_{A,3}}{\sigma_{A,1}}z_{3,2}^2\right) \leq \sigma_{B,2}\sigma_{A,2} \quad (36)$$

from which:  $z_{2,2} = \pm 1, z_{3,2} = 0$ . Plus, we also require  $z_{2,3} = 0, z_{3,3} = 0$ , since  $\mathbf{Z}$  is orthogonal.

This leads to the eight possible solutions:  $\mathbf{Z}=\mathbf{P}$ , which proves the theorem.

## VI.Acknowledgments

The author is highly indebted to Dr Marco Zannoni, for his valuable advices and fruitful discussions on perspective geometry and matrix algebra.

## VII.References

- [1] Wabha, G., "A Least Squares Estimate for Spacecraft Attitude," *SIAM Review*, Vol. VII, No. 3, p. 409-409, 1965.  
<https://doi.org/10.1137/1007077>
- [2] Markley, F.L., "Attitude determination using vector observations and the singular value decomposition," *Journal of the Astronautical Sciences* Vol. 36, No. 3, 1988, pp. 245–258.
- [3] Hotovy, S. G., "Horizon Sensor Models", *Spacecraft Attitude Determination and Control*, edited by J. R. Wertz, 1<sup>st</sup> ed., Kluwer Academic Publishers, The Netherlands, 1978, pp. 230-237. doi:10.1007/978-94-009-9907-7
- [4] Liebe, C. C., "Star trackers for attitude determination," *IEEE Aerospace and Electronic Systems Magazine*, Vol. 10, No. 6, 1955, pp. 10-16. doi: 10.1109/62.387971.
- [5] Delabie, T., De Schutter, J., and Vandenbussche, B., "Highly Efficient Attitude-Estimation Algorithm for Star Trackers Using Optimal Image Matching", *Journal of Guidance, Control, and Dynamics*, Vol. 36, No. 6, 2013, pp. 1672-1680. <https://doi.org/10.2514/1.61082>
- [6] Bevilacqua, A., Bianchi, C. Carozza, L., Gherardi, A., Melega, N., Modenini, D. and Tortora, P., "Standalone Three-Axis Attitude Determination from Earth Images", *Advances in the Astronautical Sciences*, Vol. 136, pp. 695-714, 2010.
- [7] Hartley, R., and Zisserman, A., "Action of a projective camera on quadrics", *Multiple View Geometry in Computer Vision*, 2<sup>nd</sup> ed., Cambridge University Press, New York, 2004, pp. 201-202.  
<https://doi.org/10.1017/CBO9780511811685>

- [8] Markley, F. L. and Crassidis, J. L., "Matrix Solutions of Wahba's Problem", *Fundamentals of Spacecraft Attitude Determination and Control*. Springer, New York, 2014, pp. 196-197. doi:10.1007/978-1-4939-0802-8
- [9] Ziou, D. and Tabbone, S., "Edge detection techniques: An overview," *International Journal of Pattern Recognition and Image Analysis*, Vol. 8, No. 4, 1998, pp. 537–559.
- [10] Gander, W., Golub, G.H. and Strebel, R., "Least-squares fitting of circles and ellipses," *BIT Numerical Mathematics*, Vol.34, No. 4, 1994, pp. 558–578. <https://doi.org/10.1007/BF01934268>
- [11] Taubin, G., "Estimation of planar curves, surfaces, and nonplanar space curves defined by implicit equations with applications to edge and range image segmentation," *IEEE Transactions on Pattern Analysis and Machine Intelligence*, Vol. 13, No. 11, 1991, pp. 1115-1138. doi: 10.1109/34.103273
- [12] Mortari, D., de Dilectis, D., and Zanetti, R., "Position Estimation Using the Image Derivative", *Aerospace*, Vol. 2, No. 3, 2015, pp. 435-460. doi:10.3390/aerospace2030435
- [13] Kopp, J., Efficient numerical diagonalization of Hermitian 3 x 3 matrices. *International Journal of modern Physics C*, Vol.19, No. 3, 2008, pp. 523–548. <https://doi.org/10.1142/S0129183108012303>
- [14] Wark, D. Q., Alishouse, J., and Yamamoto, G., "Variation of the Infrared Spectral Radiance near the Limb of the Earth," *Applied Optics* Vol. 3, 1964, pp. 221–227. <https://doi.org/10.1364/AO.3.000221>
- [15] Jalink, A., Davis, R. E., and Dodgen, J. A., *Conceptual Design and Analysis of an Infrared Horizon Sensor with Compensation for Atmospheric Variability*. NASA TN D-6616, 1972.
- [16] Szpak, Z. L., Chojnacki, W., van den Hengel, A., "Guaranteed ellipse fitting with a confidence region and an uncertainty measure for centre, axes, and orientation," *Journal of Mathematical Imaging and Vision*, Vol. 52, No. 2, 2015, pp 173–199. <http://dx.doi.org/10.1007/s10851-014-0536-x>